PCCP

PAPER

View Article Online
View Journal | View Issue

Cite this: *Phys. Chem. Chem. Phys.*, 2016, **18**, 27808

The first example of *ab initio* calculations of f–f transitions for the case of $[Eu(DOTP)]^{5-}$ complex—experiment *versus* theory†

Rafał Janicki,*[a] Andrzej Kędziorski*[b] and Anna Mondry[a]

Received 29th July 2016,
Accepted 12th September 2016

DOI: 10.1039/c6cp05284c

www.rsc.org/pccp

Crystal structures and photophysical properties (IR and UV-vis-NIR) of two compounds, $[C(NH_2)_3]_5[Eu(DOTP)]\cdot 12.5H_2O$ and $K_5[Eu(DOTP)]\cdot 11H_2O$ (DOTP = 1,4,7,10-tetraazacyclododecane-1,4,7,10-tetrakis (methylenephosphonic acid)), were determined. The DOTP ligand is bonded to Eu^{3+} *via* four O and four N atoms, filling thus eight coordination sites of Eu^{3+}. The experimental structures of two $[K_4Eu(DOTP)]^-$ clusters were used as a starting point for theoretical *ab initio* calculations based on a multireference wavefunction approach. Positions of the energy levels of the $4f^6$ configuration of the Eu^{3+} ion have been calculated and compared with those derived from the experimental spectra. This enabled us to tentatively assign energy levels of the Eu^{3+} ion. The relationship between calculated energies of excited states and Eu–N and Eu–O bond lengths was discussed with respect to the nephelauxetic effect.

1. Introduction

Lanthanide complexes with polydendate amino acids, which are based on the cyclen backbone (1,4,7,10-tetraazacyclododecane), are of considerable interest at present, since Gd–DOTA (DOTA = 1,4,7,10-tetraazacyclododecane-1,4,7,10-tetraacete ligand) and Tm–DOTP complexes were found to be useful in medical and biological diagnostics.[1] The Gd–DOTA complex serves as a MRI contrast agent while Tm–DOTP has been used as a NMR effective shift reagent and extracellular space marker.[2] Ligand modifications consisting of carboxylic or phosphonic arms substitution by an aromatic group may expand the applications of such complexes as potential multifunctional luminescence bioprobes[3] and single molecular magnets.[4] In this context the Ln–DOTA and Ln–DOTP systems may be considered as model compounds. From this point of view, the physicochemical properties in relation to theoretical study are of utmost importance in designing compounds in new applications. It is worthwhile noting that the diversity of potential applications for this class of compounds is related to the presence of incompletely filled 4f orbitals, which are only slightly disturbed by the ligand field. This is a reason why *ab initio* calculations of lanthanide systems are not straightforward—they have to include electron correlation and relativistic effects simultaneously.[4b] Addressing the theoretical *ab initio* study to such group of compounds is of particular interest. For example, the *ab initio* calculations of the lowest energy levels of Dy–DOTA complex have already been performed in the context of its magnetic properties.[4b,c] Comparison of the results for such calculations with the experimental ones may verify the quality of the former. On the other hand, theoretical results may provide additional information about a particular system that cannot be extracted from the experiment. However, it should be pointed out that many theoretical studies devoted to structural properties of lanthanide molecular complexes have already been completed using density functional theory (DFT).[5] In such an approach it is very common to represent the open 4f shell of the lanthanide ion by effective core pseudopotential due to computational savings and the inability of DFT methods to describe properly the highly localized and correlated f-electrons. Furthermore, the semi-empirical analysis of energy levels based on crystal-field theory needs *a priori* assumptions about the assignment of energy levels, which in low-symmetry systems is ambiguous and also suffers from the large number of adjustable parameters.[6]

This paper focuses on the experimental and *ab initio* theoretical study of the $[Eu(DOTP)]^{5-}$ complex in single crystals of the following formulas: $[C(NH_2)_3]_5[Eu(DOTP)]\cdot 12.5H_2O$ and $K_5[Eu(DOTP)]\cdot 11H_2O$. Only two crystal structures of monomeric

[a] *University of Wrocław, Faculty of Chemistry, Address F. Joliot-Curie 14, 50-383 Wrocław, Poland. E-mail: rafal.janicki@chem.uni.wroc.pl*
[b] *Nicolaus Copernicus University, Faculty of Physics, Astronomy and Informatics, Address Toruń, Institute of Physics, Poland. E-mail: andrzej.kedziorski@fizyka.umk.pl*

† Electronic supplementary information (ESI) available: Table S1. The assignments of the selected vibrations in IR spectra of **I** and **II**, Table S2. Theoretical energies (in cm^{-1}) $^{2S+1}L_J$ states of $\mathbf{II}_{Eu1}$ and $\mathbf{II}_{Eu2}$ obtained within CASSCF/CASPT2/RASSI calculations. Table S3. Cartesian coordinates (in Å) of the DFT optimized geometry of $\{K_4[Eu(DOTP)]\}^-$ cluster representing $\mathbf{I}_{Eu1}$ and $\mathbf{II}_{Eu1}$ sites. CCDC 1484638 and 1484639. For ESI and crystallographic data in CIF or other electronic format see DOI: 10.1039/c6cp05284c

Ln–DOTP complex (Ln = Gd, Tm) have been reported[7,8] and neither spectroscopic properties of monocrystals nor theoretical *ab initio* calculations have been described thus far. Theoretical calculations are performed for the two clusters $\{K_4[Eu(DOTP)]\}^-$ representing two different Eu sites for the $K_5[Eu(DOTP)]\cdot 11H_2O$ crystal. Energies of the excited states for the $4f^6$ configuration were obtained within the quantum chemistry *ab initio* methods based on the multireference wave-function approach, which allows accounting for static and dynamic electron correlation as well as relativistic effects.

2. Results and discussion

2.1 Crystal structures

The $[Eu(DOTP)]^{5-}$ complex crystallizes in the form of compounds of the following formulas: $[C(NH_2)_3]_5[Eu(DOTP)]\cdot 12.5H_2O$ (hereinafter **I**) and $K_5[Eu(DOTP)]\cdot 11H_2O$ (hereinafter **II**). The crystals of **I** are monoclinic and belong to the *P*2/*n* space group while those of **II** crystallize in the tetragonal system (*P*4*cc* space group). The crystals of **I** comprise $[Eu(DOTP)]^{5-}$ complexes, guanidinium cations and water molecules, while **II** consist of $[Eu(DOTP)]^{5-}$ complexes, potassium cations and lattice water molecules. In both compounds the $[Eu(DOTP)]^{5-}$ complex anions are deprotonated and their negative charge is compensated by $[C(NH_2)_3]^+$ (in **I**) or K^+ (in **II**) cations. The $[DOTP]^{8-}$ ligand is bonded to the Eu^{3+} cation by four oxygen and four nitrogen atoms, filling thus eight coordination places of the Eu^{3+} cation. Both structures contain two symmetry-independent $[Eu(DOTP)]^{5-}$ anions that differ in the conformation of the DOTP ligand, giving rise to two enantiomers $\Lambda(\lambda\lambda\lambda\lambda)$ (hereinafter $\mathbf{I_{Eu1}}$, $\mathbf{II_{Eu1}}$) and $\Delta(\delta\delta\delta\delta)$ (hereinafter $\mathbf{I_{Eu2}}$, $\mathbf{II_{Eu2}}$). The molecular structures of $[Eu(DOTP)]^{5-}$ anions are presented in (Fig. 1).

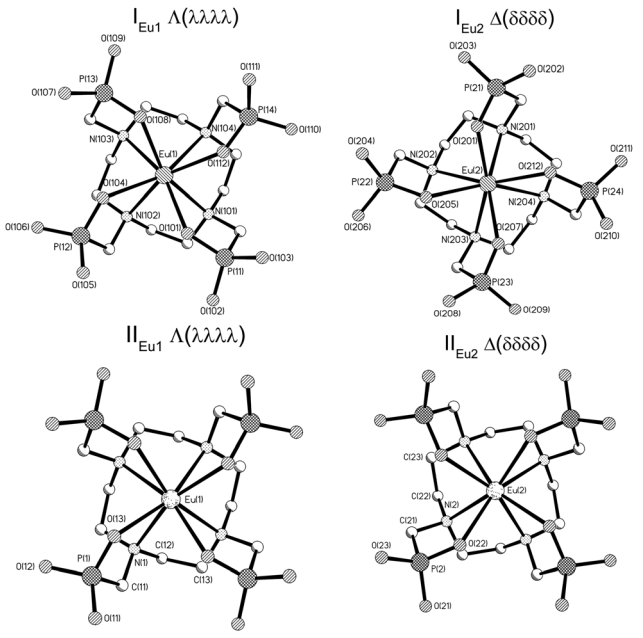

Fig. 1 Molecular structures of $[Eu(DOTP)]^{5-}$ anions in **I** and **II**.

Table 1 Selected Ln–O and Ln–N bond lengths for crystals under study and for Gd–DOTP[7] and Tm–DOTP[8] complexes

$\mathbf{I_{Eu1}}$	Eu1–O108	2.321(3)	Eu1–N102	2.679(3)
	Eu1–O104	2.339(3)	Eu1–N101	2.677(3)
	Eu1–O112	2.331(3)	Eu1–N104	2.710(3)
	Eu1–O101	2.338(3)	Eu1–N103	2.706(3)
$\mathbf{I_{Eu2}}$	Eu2–O201	2.294(3)	Eu2–N201	2.646(3)
	Eu2–O207	2.328(3)	Eu2–N203	2.696(3)
	Eu2–O205	2.343(3)	Eu2–N202	2.698(3)
	Eu2–O212	2.342(3)	Eu2–N204	2.721(3)
$\mathbf{II_{Eu1}}$	Eu1–O13	2.325(4)	Eu1–N1	2.732(5)
$\mathbf{II_{Eu2}}$	Eu2–O22	2.346(4)	Eu2–N2	2.705(5)
I	**Eu–O$_{av}$**	**2.330(16)**	**Eu–N$_{av}$**	**2.691(24)**
II	**Eu–O$_{av}$**	**2.336(15)**	**Eu–N$_{av}$**	**2.719(19)**
	Gd–O$_{av}$	**2.314(1)**	**Gd–N$_{av}$**	**2.660(10)**
	Tm–O$_{av}$	**2.26(1)**	**Tm–N$_{av}$**	**2.63(1)**

Selected Eu–O and Eu–N bond lengths are presented in Table 1. The average Ln–O and Ln–N distances in the case of Gd–DOTP and Tm–DOTP complexes are also presented in the table for comparison purposes.[7,8]

Respective Eu–O and Eu–N distances for both isomers in **I** are similar. However, there are two exceptions—namely, Eu2–O201 and Eu2–N201 bond lengths in **I** are significantly shorter. For this reason the structure of the $\mathbf{I_{Eu2}}$ enantiomer is more distorted than the $\mathbf{I_{Eu1}}$ one.

Average Eu–O and Eu–N distances are longer compared to those determined for $[Gd(DOTP)]^{5-}$ and $[Tm(DOTP)]^{5-}$ complexes.[7,8] This is brought about by the lanthanide contraction.

The coordination polyhedra in **I** and **II** may be described as twisted square antiprism (TSAP), in which the corners are occupied by four O atoms (O_{IV} – plane) and four N atoms (N_{IV} – plane). In **I** the O_{IV} and N_{IV} planes are almost parallel to each other, with the dihedral angle between them equal to 0.6° and 0.9° in enantiomers $\mathbf{I_{Eu1}}$ and $\mathbf{I_{Eu2}}$, respectively. In **II** both O_{IV} and N_{IV} planes are perfectly parallel owing to the fact that the Eu^{3+} ion is located in fourfold axes. The twist angles of rectangles formed by four O_{IV} atoms as well as by four N_{IV} atoms in **I** and **II** are schematically presented in Fig. 2a.

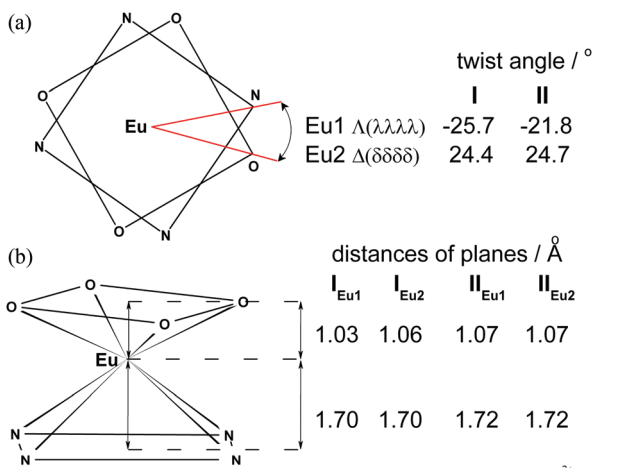

Fig. 2 (a) Twist angle and (b) schematic coordination polyhedron and distances of Eu^{3+} from O_{IV} and N_{IV} planes.

Table 2 Distances (Å) between closest water molecule and Eu^{3+} cation in **I** and **II**

I		**II**	
Eu1–OW1	4.388	Eu1–OW4	4.181
Eu2–OW2	4.360	Eu2–OW1	4.029

The small twist angle values between the O_{IV} and N_{IV} planes and the absence of a water molecule in the first coordination sphere of Eu^{3+}, indicate that the crystals contain a minuscule type of the m′ isomer as a racemic mixture of two $\Lambda(\lambda\lambda\lambda\lambda)$ and $\Delta(\delta\delta\delta\delta)$ enantiomers. The average distances between O_{IV} and N_{IV} planes are similar in both crystals and range from 2.73 Å to 2.79 Å. The Eu^{3+} cation is located inside the square antiprism at a distance of 1.03–1.07 Å to O_{IV} and 1.70–1.72 Å to N_{IV} planes (Fig. 2b).

All phosphonic groups are deprotonated; thus the P–O bond lengths are similar and range from 1.508(4) Å to 1.550(5) Å. The average P–O bond length is equal to ~1.527(8) Å, and is very close to those found in other lanthanide aminophosphonates such as Ln–EDTMP and Ln–CDTMP.[9,10]

There are no water molecules coordinated to Eu^{3+} in the $[EuDOTP]^{5-}$ complexes in **I** and **II**, while in its carboxylic analogue, $[Eu(DOTA)(H_2O)]^-$, one water molecule is directly bonded to the Eu^{3+} ion.[11] The absence of the water molecule in the closest neighbourhood of $[Eu(DOTP)]^{5-}$ is likely caused by the spherical hindrance connected with an accumulation of highly negative phosphonic oxygen atoms, which strongly repels water molecules and prevents their coordination to Eu^{3+}. The water molecules were found in the second coordination sphere of $[Eu(DOTP)]^{5-}$ complex. The nearest H_2O molecule is about 4 Å from the Eu^{3+} cation as shown in Table 2.

Similar interaction of water molecules from the second sphere was observed in the case of the Ho–DOTMA complex (where DOTMA is 1R,4R,7R,10R-α,α′,α″,α‴-tetramethyl-1,4,7,10-tetraazacyclo-dodecane-1,4,7,10-tetraacetic acid).[12] Weak interaction of outer-sphere water molecules with $[Ln(DOTP)]^{5-}$ anions is probably a reason of high relaxivity of the $[Gd(DOTP)]^{5-}$ system.[13]

Distortion of the $[Eu(DOTP)]^{5-}$ complex in **I** brings about its symmetry that is approximately C_4, while in **II** the complex's symmetry is exact (C_4) because it is imposed by crystallographic fourfold axes.

Taking into account the structural variations of the $[Eu(DOTP)]^{5-}$ complex in **I** and **II**, the question that arises is how they are reflected in the IR and UV-vis spectra of both crystals.

2.2 IR spectroscopy

The IR spectra of both compounds were measured and the theoretical IR spectra of $\{K_4[Eu(DOTP)]\}^-$ clusters representing $\mathbf{II_{Eu1}}$ and $\mathbf{II_{Eu2}}$ sites were obtained within the DFT approach for the B3LYP exchange–correlation functional. Because the theoretical DFT calculations were performed for isolated the $\{K_4[Eu(DOTP)]\}^-$ anion (C_1 symmetry) in the simulated spectra, there are no bands attributed to internal vibrations of water molecules and guanidinium cations. The complex anion $\{K_4[Eu(DOTP)]\}^-$ contains 61 atoms giving rise to 177 fundamental

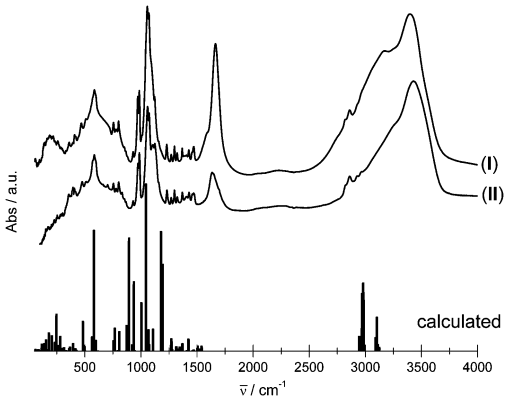

Fig. 3 Experimental and theoretical IR spectra of compounds under study.

vibrations that may be decomposed into 45A + 44B + 44E, where A, B and E denote irreducible representations of the C_4 point group. Owing to the selection rules, all A → B fundamental excitations are forbidden in the IR spectra. The spectra of crystals under study are presented in Fig. 3. As seen here the spectral features of both crystals are similar. Theoretical study results enabled us to assign the bands observed in the experimental spectrum (see Table S1, ESI†).

The main differences between the experimental spectra of both compounds are observed for bands located between 1490 cm^{-1} and 4000 cm^{-1}. In this spectral range, the broad bands centered at ~1630 cm^{-1} and ~3425 cm^{-1} are attributed to the δ_{OH_2} and ν_{OH} vibrations, respectively, from the lattice water molecules. The δ_{OH_2} band in the **I** spectrum is partly covered by the intense δ_{NH_2} band from the guanidine cations. Certain differences appear in the spectral pattern of bands centered at ~1070 cm^{-1}. These bands are ascribed to ν_{POsym} and ν_{POasym}. In general, splitting and shape changes of the ν_{PO} bands reflect various geometrical changes of phosphonic groups as shown previously.[9] The bands attributed to the Eu–O and Eu–N vibrations are located below 450 cm^{-1}.

Observed similarities of the spectral features of **I** and **II** strongly suggest that the geometry of $[Eu(DOTP)]^{5-}$ complexes is substantially the same. Therefore, it seems to be justified to consider the local symmetry of both complex anions as C_4 in spite of the fact that there is some certain deformation of $[Eu(DOTP)]^{5-}$ complex in **I**.

2.3 UV-vis electronic spectroscopy

The UV-vis absorption $^7F_0 \rightarrow {}^5D_J$ (J = 0, 1, 2, 3, 4),$^5L_6$ and luminescence $^5D_0 \rightarrow {}^7F_J$ (J = 0, 1, 2, 3, 4, 5, 6) spectra of crystals, recorded at RT in the spectral region 14 000–28 000 cm^{-1} are shown in Fig. 4 and 5, respectively.

Experimental absorption spectra consist of narrow bands attributed to transitions from the ground $^7F_0$ state to the excited levels of the $4f^6$ configuration. The experimental emission spectra comprise bands corresponding to transitions from the excited $^5D_0$ state to lower-lying ^7F_J levels (where J = 0, 1, 2, 3, 4, 5, 6). Mechanisms of the electric-dipole f–f transitions, where J = 0–J' = 2, 4, 6, observed in Eu^{3+} materials can be described *via* standard Judd–Ofelt theory,[14,15] whereas the

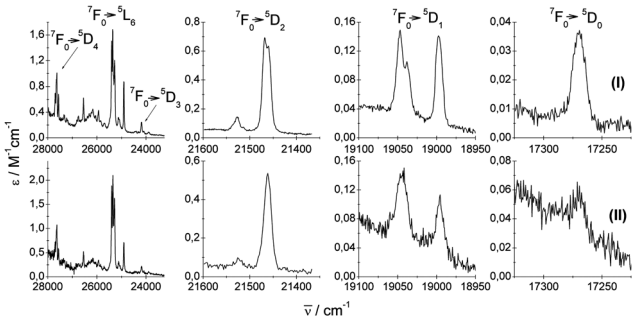

Fig. 4 Experimental (**I** and **II**) UV-vis absorption $^7F_0 \rightarrow {}^5D_{J=0,1,2,3,4}, {}^5L_6$ spectra of crystals under study.

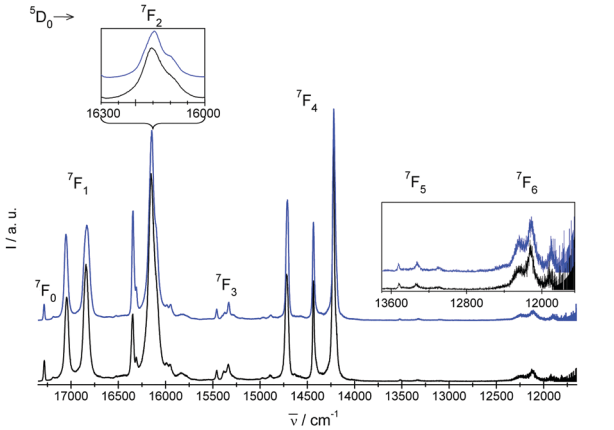

Fig. 5 Experimental emission $^5D_0 \rightarrow {}^7F_{J=0,1,2,3,4,5,6}$ spectra of crystals under study. **I** = blue and **II** = black.

electric-dipole $J = 0$–$J' = 0, 3, 5$ demands extended theory.[16,17] $^7F_0$–$^5D_1$ and $^5D_0$–$^7F_1$ transitions are of magnetic dipole character. The $\Delta S = 0$ selection rule for both electric- and magnetic-dipole transitions is relaxed *via* the spin–orbit interaction within the lanthanide ion. Now, consider the selection rules from the point of view of the local symmetry of the europium crystallographic site.

In the case of the Eu^{3+} cation, both ground ($^7F_0$) and emission excited ($^5D_0$) states are fully symmetric. According to group theory, the A ↔ A,E electronic-dipole and magnetic-dipole transitions between the crystal field (CF) states are allowed in the C_4 symmetry; at the same time, the A ↔ B transitions are forbidden. The numbers of spectral lines expected for Eu^{3+} ion in the site of C_4 symmetry are collected in Table 3 along with the total numbers of experimentally observed lines in the absorption and emission spectra of **I** and **II**.

In most cases, the experimental number of observed spectral lines is smaller compared to the theoretical prediction. We were unable to separate CF levels of individual Eu sites. To unequivocally assign the bands observed in the spectra of **I** and **II**, the analysis was extended into theoretical calculations.

2.4 Theoretical energy levels

The *ab initio* calculations of energies of the $\mathbf{II_{Eu1}}$ and $\mathbf{II_{Eu2}}$ complexes were performed in the following steps:

Table 3 Number of spectral lines predicted from group theory and those observed in **I** and **II**

			Absorption spectra $^7F_0 \rightarrow {}^{2S+1}L_J$		Luminescence spectra $^5D_0 \rightarrow {}^7F_J$	
J	C_4 symmetry		**I**	**II**	**I**	**II**
0	A	1	1	1	1	1
1	A + E	2	2	2	2	2
2	A + 2·B + E	2	3[a]	2	3[b]	3[b]
3	A + 2·B + 2·E	3	3	3	3	3
4	3·A + 2·B + 2·E	5	4	3	4	4
5	3·A + 2·B + 3·E	6			4	4
6	3·A + 4·B + 3·E	6			3	3

[a] C_4 symmetry of **I** is not exact, thereby allowing larger number of spectral lines than expected for C_4 symmetry. [b] Line at 16 400 cm^{-1} in Fig. 5 finally interpreted as of cooperative vibronic origin was taken into account here.

- complete active space self-consistent field method (CASSCF)[18]
- complete active space perturbation theory of second-order (CASPT2)[19,20]
- restricted active space state interaction (RASSI)[21]

CASSCF and CASPT2 methods account for non-dynamic (static) and dynamic correlation effects, respectively, whereas the RASSI one includes the spin–orbit (SO) interaction. This sequence of calculations, denoted here by CASSCF/CASPT2/RASSI-SO, was performed for the active space that corresponds to the $4f^6$ configuration of the Eu^{3+} ion. In this way the energies of ^7F and ^5D, ^5F, ^5G, ^5H, ^5I, ^5K and ^5L states were calculated within the *ab initio* approach (for details see Section 3.4). Selected experimental and theoretical energy levels are collected in Table 4. A complete list of calculated energy levels is presented in Table S2 in ESI.†

Absolute differences of the *ab initio* energies of respective levels (*vis-a-vis* $^7F_0$ ground level) between $\mathbf{II_{Eu1}}$ and $\mathbf{II_{Eu2}}$ do not exceed 82 cm^{-1}, and these differences are much lower in most pairs of states. Almost all theoretically determined energy levels with respect to $^7F_0$ ground level in $\mathbf{II_{Eu1}}$ are larger than in $\mathbf{II_{Eu2}}$. Such a relationship does not seem to be accidental if the Eu–N and Eu–O bond lengths are considered. As shown in Section 2.1, the Eu1–N1 bond length in isomer $\mathbf{II_{Eu1}}$ is about 0.039 Å longer than the Eu2–N2 in $\mathbf{II_{Eu2}}$. In the case of Eu–O bond lengths, the opposite situation is observed—the Eu1–O13 bond length is 0.026 Å shorter in $\mathbf{II_{Eu1}}$ than the corresponding Eu2–O22 in $\mathbf{II_{Eu2}}$. The obtained lowering of the energy levels of $4f^6$ of $\mathbf{II_{Eu2}}$ with respect to the $^7F_0$ level is theoretical evidence that weak donor atoms (such as N) brings about a bathochromic shift of f–f transitions. At the same time, in the case of hard, highly negatively charged O donor atoms, the reverse effect is expected such that the result reinforces the considered energy shift.

2.5 Assignment of experimental energy levels

Comparison of theoretical and experimental energy levels of **II** allowed us to tentatively assign the irreducible representations of C_4 point group to experimental energy levels of **II** (Table 4).

The ordering number preceding the symbol of the irreducible representation is added in order to uniquely identify the states

Table 4 Theoretical energies (in cm^{-1}) of septet ^7F and quintet ^5D, ^5L states of $\mathbf{II}_{\mathbf{Eu1}}$ and $\mathbf{II}_{\mathbf{Eu2}}$ with respect to $^7F_0$ ground level along with experimental energy levels obtained from UV-vis spectra of **I** and **II** at room temperature

	Experimental			$\mathbf{II}_{\mathbf{Eu1}}$ (theory)		$\mathbf{II}_{\mathbf{Eu2}}$ (theory)	
$^{2S+1}L_J$	**I**	**II**	Symmetry	Irrep	Energy/cm^{-1}	Irrep	Energy/cm^{-1}
$^7F_0$	0	0	1A	1A	0	1A	0
$^7F_1$	230	237	2A	2A	192	2A	206
	452	442	1E	1E	520	1E	507
$^7F_2$	939	934	?	2E	1091	2E	1079
	1139	1129	2E	1B	1111	3A	1107
	1180	1179	3A	3A	1116	1B	1111
				2B	1362	2B	1333
$^7F_3$	1826	1826	3E	3E	2015	3E	2006
	1915	1905	4A	4A	2043	4A	2033
				3B	2084	3B	2069
	1956	1951	4E	4E	2110	4E	2093
				4B	2138	4B	2128
$^7F_4$	2571	2563	5A	5A	2869	5A	2864
				6A	3058	6A	3048
	2848	2847	6A	5E	3064	5E	3050
			5E				
	3064	3058	6E	6E	3152	6E	3134
				5B	3216	7A	3196
	3095	3085	7A	7A	3218	5B	3200
				6B	3353	6B	3338
$^7F_5$	3760	3768	7E	7E	3993	7E	3995
	3959	3949	8E	8E	4169	8E	4158
				7B	4199	7B	4180
	4181	4160	8A	8A	4259	8A	4257
				9A	4291	9A	4282
				8B	4409	8B	4371
	4202	4198	9E	9E	4486	9E	4454
				10A	4537	10A	4503
$^7F_6$				9B	5037	9B	5066
				10B	5038	10B	5067
	5019	5015	10E	10E	5232	10E	5218
	5149	5154	11A	11A	5473	11A	5447
	5374	5366	12A	12A	5504	12A	5472
			11E	11E	5589	11E	5560
			13A	11B	5611	11B	5583
			12E	13A	5719	13A	5681
				12E	5732	12E	5691
				12B	5743	12B	5702
$^5D_0$	17 269	17 269	14A	14A	18 169	14A	18 156
$^5D_1$	18 998	18 996	15A	15A	18 896	15A	18 885
	19 038	19 045	13E	13E	18 961	13E	18 948
	19 047						
$^5D_2$	21 459	21 462	16A	16A	20 529	16A	20 512
	21 468						
				13B	20 535	13B	20 525
	21 528	21 526	14E	14E	20 581	14E	20 571
				14B	20 601	14B	20 587
$^5D_3$				15B	23 160	15B	23 144
	24 307	24 313	15E	15E	23 163	15E	23 157
				16B	23 200	16B	23 181
	24 387	24 402	16E	16E	23 210	16E	23 197
			17A	17A	23 214	17A	23 205
$^5D_4$	27 563	27 563	18A	18A	26 903	18A	26 894
			19A	19A	26 912	19A	26 904
	27 632		17E	17E	26 917	17E	26 909
				17B	26 951	17B	26 939
				18B	26 965	18B	26 953
	27 654	27 632	18E	18E	27 011	18E	26 995
	27 700	27 693	20A	20A	27 043	20A	27 026
$^5L_6$				27B	28 584	27B	28 537
	25 094	25 056	27E	27E	28 598	27E	28 555
	25 125	25 093	29A	29A	28 610	29A	28 565
				28B	28 678	28B	28 608
				29B	28 682	29B	28 618
	25 284	25 285	28E	28E	28 777	28E	28 747
	25 361	25 351	30A	29E	28 847	29E	28 808
			29E				
	25 400	25 401	31A	31A	28 911	31A	28 876
				30B	28 802	30B	28 761
				30A	28 827	30A	28 806

of the same symmetry. It is seen in Table 4 that the ordering of theoretical energy levels is almost the same in the case of $\mathbf{II}_{\mathbf{Eu1}}$ and $\mathbf{II}_{\mathbf{Eu2}}$, with the exception of two pairs—1B and 3A, energy levels of $^7F_2$ multiplet and 5B and 7A ones of $^7F_4$—where the ordering of levels is interchanged.

As seen from the theoretical results, differences between corresponding CF levels of individual $^{2S+1}L_J$ multiplets in both isomers are usually only of a few cm^{-1}. For this reason it was not possible to separate CF levels of the individual Eu sites in the experimental spectra of **I** and **II**.

In the emission spectrum of **II** there are two relatively strong spectral lines originating from $^5D_0$ level centered at 16 335 cm^{-1} and 16 140 cm^{-1} (energy separation 195 cm^{-1}). A closer look at the line at 16 140 cm^{-1} (inset in Fig. 5) shows that in fact it consists of two lines separated by 50 cm^{-1}. A similar spectral pattern is observed in the case of $^5D_0 \rightarrow {}^7F_2$ of **I**. At the same time, only two distinct lines separated by only 25 cm^{-1} and 28 cm^{-1} for $\mathbf{II}_{\mathbf{Eu1}}$ and $\mathbf{II}_{\mathbf{Eu2}}$, respectively, that originate from $^5D_0 \rightarrow {}^7F_2$(2E) and $^5D_0 \rightarrow {}^7F_2$(3A) transitions can be derived from the *ab initio* calculations. Therefore the symmetry of the CF components of the $^7F_2$ multiplet at 1129 cm^{-1} and 1179 cm^{-1} derived from the luminescence spectrum of **II** were ascribed as 2E and 3A, respectively. Despite of its relatively high intensity, the position of the line centered at 16 335 cm^{-1} matches relatively well the energy of the cooperative vibronic transition that couples the electronic $^7F_0$ state with one of the $\nu_{P\text{-}O}$ stretching vibrations of the energy ranging between 900 cm^{-1} and 1000 cm^{-1}. In this way the number of CF levels is in accordance with that predicted by the theory. Similar vibronic lines were observed in emission spectra of other Eu^{3+} complexes containing phosphonic groups,[9,22] but authors of those papers interpreted the lines as of pure electronic origin.

2.6 Experimental *versus* theoretical energies

There are two energy scales that govern the energy level schemes of ground $4f^n$ configurations of Ln^{3+} ions, namely the energy separations between barycentres of $^{2S+1}L_J$ multiplets (10^3–10^4 cm^{-1}) and the crystal field splittings (10^1–10^2 cm^{-1}) of these multiplets.

The centres of gravity of experimental (for **I** and **II**) and theoretical energy levels $^{2S+1}L_J$ are listed and compared in Table 5. The table shows that calculated energies of states are overestimated in the case of majority ^7F_J levels with the one exception of the $^7F_2$ energy level, for which the experimental energy is larger than the theoretical counterpart. The absolute differences between experimental and theoretical energies of ^7F_J states (hereinafter referred to as Δ) do not exceed 280 cm^{-1}.

Table 5 Experimental and theoretical centres of gravity, $^{2S+1}L_J$ energy levels of $4f^6$ configuration for Eu–DOTP complex in **I**, **II** and theoretical values obtained for energies listed in Table 4. Differences between the experimental and theoretical values Δ are provided in the last two columns

	Experimental		Calculations		
	I	**II**	**I** and **II**[a]	$\Delta_{\mathbf{I}\text{-calc}}$	$\Delta_{\mathbf{II}\text{-calc}}$
$^7F_1$	378	374	409	31	35
$^7F_2$	1153	1146	1094	−59	−52
$^7F_3$	1826	1826	2102	276	276
$^7F_4$	2956	2910	3085	129	175
$^7F_5$	4004	3999	4216	212	217
$^7F_6$	—	—	5464	—	—
$^5D_0$	17 269	17 269	18 163	894	894
$^5D_1$	19 028	19 029	18 933	−95	−96
$^5D_2$	21 505	21 505	20 558	−947	−947
$^5D_3$	24 360	24 372	23 210	−1150	−1162
$^5D_4$	27 639	27 601	26 953	−686	−648
$^5L_6$	25 195	25 214	28 737	3542	3523

[a] Theoretical values are averaged over the SA-CASSCF/MS-CASPT2/RASSI-SO energies obtained for both sites $\mathbf{II}_{\mathbf{Eu1}}$ and $\mathbf{II}_{\mathbf{Eu2}}$.

Direct comparison of theoretical energies for the excited states with respect to the $^7F_0$ ground level with experimental counterparts shows that they may differ even by thousands of cm^{-1}, reaching 3500 cm^{-1} for the $^5L_6$ level. Such discrepancies are expected in the case of many-electron systems in which electron correlation and relativistic effects are important. Theoretical studies for the CaF_2:Pr^{3+} case have shown that discrepancies in energy calculations of free lanthanide ions are transferred to more complex systems containing lanthanide ions.[23] To illustrate this problem we have performed similar CASSCF/CASPT2/RASSI-SO calculations for the Eu^{3+} free ion that were compared with energy levels of the experimental Eu^{3+} aqua ion[24] as presented in Table 6. Energy levels of Eu^{3+} free ion calculated within the Dirac–Fock multiconfiguration interaction approach (MCDF-CI)[25] are presented in Table 6. More recently the *ab initio* calculations within fully relativistic Kramers pairs configuration interaction method for free Eu^{3+} ions as well as for aqua ions were reported.[26]

Table 6 Experimental (Eu^{3+} aqua ions[24]) and theoretical energies of $4f^6$ configuration of Eu^{3+} free ion. Energies are provided with respect to the ground energy level $^7F_0$. In this work the energies were calculated within CASSCF/CASPT2/RASSI approach active space corresponding to $4f^6$ configuration

	Energy/cm^{-1}				
$^{2S+1}L_J$	Experimental[24]	MCDF-CI[25]	ΔE	This work	ΔE
$^7F_1$	360	347	−13	395	35
$^7F_2$	1020	965	−55	1115	95
$^7F_3$	1887	1775	−112	2049	162
$^7F_4$	2865	2712	−153	3095	230
$^7F_5$	3908	3735	−173	4203	295
$^7F_6$	4980	4810	−170	5387	407
$^5D_0$	17 277	18 857	1580	17 733	456
$^5D_1$	19 028	20 504	1476	18 499	−529
$^5D_2$	21 519	22 896	1377	20 119	−1400
$^5D_3$	24 408	25 728	1320	22 744	−1664
$^5L_6$	25 400	28 178	2778	28 405	3005
$^5D_4$	27 632	29 135	1503	26 545	−1087

The experimental energy levels of the Eu^{3+} free ion are not known to the authors. At the same time the aqua ion seems to be the system reasonably ''similar'' to the free ion; for example, it is interesting to note that the experimentally observed Eu^{3+} aqua ion energy levels[24] are very close to those interpolated to approach the Eu^{3+} free ion ones.[27] Comparison of the performance of the present theoretical approach with the benchmark MCDF-CI calculations presented in Table 6 shows that the discrepancies with respect to the experiment of the order of thousands of cm^{-1} is what one can expect from *ab initio* calculations performed for the Eu^{3+} ion. Furthermore, similarities of the energy differences between the CASSCF/CASPT2/RASSI-SO calculations and experimental counterparts presented in Tables 5 and 6 support the conclusion that the main deficiencies in the proper theoretical description of f-electron systems are due to insufficient accounting for correlation effects within the lanthanide ion. For example, detailed analysis of radial correlation effects in free lanthanide ions based on *ab initio* calculations was performed by Barandiaran and Seijo.[28] Their study indicated that the most probable improvement of the description of energies for excited states of heavy lanthanide ions—for example, of Eu^{3+}—was obtained by inclusion of 5f orbitals into the active space. However, such enlargement of the active space in the case of considered (large) Eu–DOTP complexes is not tractable with the authors' available computational resources.

The other energy scale is associated with splitting of the $^{2S+1}L_J$ energy levels in the crystal field potential. Absolute values of differences between the theoretical and experimental crystal field splittings—that is, splittings of $^{2S+1}L_J$ levels—do not exceed the value of 220 cm^{-1}; this maximum discrepancy is observed within $^5L_6$ multiplets and can be derived from Table 4. However, it should not be interpreted as the crystal field splittings being much better described within CASSCF/CASPT2/RASSI-SO approach than positions of levels with respect to the energy of the ground state $^7F_0$. Rather, it is attributed to the fact that differences between theoretical and experimental energies follow the scale of considered energies. Namely, upon considering relative energy differences, then it would turn out that the relative differences are larger in the case of crystal field splittings.

2.7 $^5D_0 \rightarrow {}^7F_0$ transition energy

Among the f–f transitions observed in the electronic spectra of Eu^{3+}, the $^7F_0 \leftrightarrow {}^5D_0$ transition is the most suitable for a study of Eu–ligand interaction. The ground $^7F_0$ and the excited $^5D_0$ states are non-degenerated and do not split in the crystal field of any symmetry. Therefore, the number of components observed in the spectrum of this transition indicates the minimal number of chemically distinct environments of the Eu^{3+} ion.

The energy of the $^7F_0 \rightarrow {}^5D_0$ transition is also used to study the nephelauxetic effect of europium compounds. This effect is probably connected with the covalent contribution to the bonding between the Eu^{3+} ion and the ligands, metal–ligand distances, coordination numbers and the total charge and acid base properties of ligands bonded with Eu^{3+}.[29] However, there is no simple correlation between the energy of the $^7F_0 \rightarrow {}^5D_0$ transition and these physical quantities.[30] Bathochromic shifts

of the $^7F_0 \rightarrow {}^5D_0$ band are very often explained as resulting from the change in the interelectronic repulsion Slater F^k parameters of Eu^{3+} ion in the ligand field with respect to those for the free ion $\left(\beta = \frac{F^k_{\text{complex}}}{F^k_{\text{free ion}}}\right)$.[31] In general in the case of the rare earth complexes for which the semi-empirical values of the F^k parameters of the free ions are not known, the nephelauxetic ratio is approximated as $\beta = \frac{\overline{\nu}_{^7F_0 \rightarrow {}^5D_0\ \text{complex}}}{\overline{\nu}_{^7F_0 \rightarrow {}^5D_0\ \text{aqua ion}}}$, where $\overline{\nu}_{^7F_0 \rightarrow {}^5D_0\ \text{complex}}$ and $\overline{\nu}_{^7F_0 \rightarrow {}^5D_0\ \text{aqua ion}}$ are the wavenumbers of the $^7F_0 \rightarrow {}^5D_0$ bands for the complex and the aqua ion, respectively.

Present work allows for the direct calculation of the nephelauxetic ratios. All the nephelauxetic ratios β calculated using the formula with F^k radial integrals (obtained within the *ab initio* approach) are equal to about 0.99. Radial 4f functions used for calculating Slater radial integrals were extracted from the molecular orbitals of $\mathbf{II_{Eu}}$ and Eu^{3+} free ions obtained within the CASSCF method. Details of calculations for radial integrals based on molecular orbitals will be presented elsewhere.[32] The result that the values of β are close to unity supports the ionic character of Eu–L interaction. Furthermore, the nephelauxetic ratios β are smaller than unity, which is expected from the point of view of the nature of the nephelauxetic effect.

It is worth stressing that the energy of the $^7F_0 \rightarrow {}^5D_0$ transition of $[Eu(DOTP)]^{5-}$ (17 269 cm^{-1}) and Eu^{3+} aqua ion (17 277 cm^{-1})[24] differs by 6 cm^{-1} only. Usually, for eight-coordinated Eu^{3+} complexes, the shift of the $^7F_0 \rightarrow {}^5D_0$ band to the lower energies in relation to the aqua ion is much larger. The opposite relation is obtained in the CASSCF/CASPT2/RASSI-SO approach, where the energy of the $^5D_0$ level with respect to $^7F_0$ ground state of free Eu^{3+}, 17 733 cm^{-1}, is smaller than the $^7F_0 \rightarrow {}^5D_0$ transition energies obtained for $\mathbf{II_{Eu1}}$ and $\mathbf{II_{Eu2}}$, 18 169 cm^{-1} and 18 156 cm^{-1}, respectively. At first glance it may be considered as being in contradiction to the result of the *ab initio* calculations that $\beta < 1$. However, the fact that the theoretical free ion $^7F_0 \rightarrow {}^5D_0$ transition energy is smaller than that of the Eu–DOTP complex probably can be ascribed to the effect of the crystal-field upon the lowest ^7F_J levels.[33] Unfortunately, the preliminary analysis within the crystal field approach has not succeeded in clarifying this problem.

2.8 Conclusions

Structural, spectroscopic and theoretical studies of two monocrystals, namely $[C(NH_2)_3]_5[Eu(DOTP)]\cdot 12.5H_2O$ and $K_5[Eu(DOTP)]\cdot 11H_2O$, were performed. Both compounds contain $[Eu(DOTP)]^{5-}$ complex in the form of minor m′ ($\Lambda(\lambda\lambda\lambda\lambda)$ and $\Delta(\delta\delta\delta\delta)$) isomers. The $[DOTP]^{8-}$ ligand is bonded to the Eu^{3+} cation *via* four oxygen and four nitrogen atoms, thereby filling eight coordination places of Eu^{3+} cations. Symmetry of the $[Eu(DOTP)]^{5-}$ complexes in the **II** crystal are of C_4, whereas their structures are slightly disrupted in the case of **I** crystal resulting in C_1 symmetry. It is found that the closest outer sphere water molecule is 4.374(20) Å and 4.105(107) Å away from the Eu^{3+} in **I** and **II**, respectively. This weak interaction of outer-sphere water molecules with $[Ln(DOTP)]^{5-}$ anions, is probably one of the reasons for high relaxivity of the $[Gd(DOTP)]^{5-}$ system in MRI.

Using available spectroscopic techniques, it was not possible to distinguish the spectral lines coming from two Eu sites existing in both crystals. Therefore, results of *ab initio* calculations allowed us to assign the spectral lines tentatively to particular crystal field components of the energy levels for the $4f^6$ configuration of the Eu^{3+} ion.

Differences between theoretical and experimental values of the energies of Eu–DOTP complexes can reach about 3500 cm^{-1}, as observed in the case of $^5L_6$ energy levels. At the same time the structure of Eu–DOTP energy levels is retained strictly up to $^5D_3$ energy levels. Such calculations are of general interest because it is possible to conclude that the correlation between structure and spectroscopic features is by its very nature discrete for the case of lanthanide systems.

The correlation between Eu–ligand bond lengths and energies of excited energy levels is obtained. It was shown that weak donor atoms (such as N) bring about the bathochromic shift of f–f transitions and reverse hard, highly negatively charged O donor atoms reinforcing the energy shift.

Discrepancies between theoretical and experimental values of energies of states for the $4f^6$ configuration of Eu^{3+} ion can be mainly attributed to treatment of correlation effects in the Eu–DOTP complex in the present *ab initio* approach. Considering the details of CASSCF/CASPT2/RASSI-SO calculations and results of other *ab initio* calculations,[24] it may be concluded that theoretical energies are expected to be improved *via* inclusion of the "double f-shell" into the CASSCF/CASPT2/RASSI-SO approach, which means that the radial correlation between 4f and 5f shells is treated in a non-perturbative way. In the present work this correlation effect was taken into account perturbatively within the CASPT2 method.

To summarize, the experimental and theoretical properties of Eu–DOTP complex were studied and discussed in detail. Although there are some discrepancies between experimental and theoretical results, the presented results enabled us to calculate the energies of $4f^6$ configuration of Eu^{3+} in molecular $[EuDOTP]^{5-}$ complex, for the first time. It is worth noting that the energies of the lower lying ^7F_J states are relatively well described.

The energies of the ^7F_J states are particularly important from the application point of view of Eu^{3+} compounds as luminescent materials, since the emission spectra of Eu^{3+} usually consist of $^5D_0 \rightarrow {}^7F_J$ lines. Another important aspect of the $[EuDOTP]^{5-}$ spectra is connected with the f–f transition intensities, therefore our future study will be focused on this problem.[34]

3. Experimental section

3.1 Preparation of crystals

Two samples each of which contained a suspension of Eu_2O_3 (0.250 g, Stanford Materials) and H_8DOTP (0.75 g, Macrocyclics) in 25 ml of H_2O were heated at *ca.* 80 °C. Next, a small portion of $[C(NH_2)_3]_2CO_3$ was added to the first one and KOH to the other until the precipitate was dissolved. The final pH of solutions was 7.5. Solutions were filtrated and left for crystallization.

Colourless crystals of $[C(NH_2)_3]_5[Eu(DOTP)]\cdot 13H_2O$ and $K_5[Eu(DOTP)]\cdot 11H_2O$ were formed during very slow evaporation of water after s few months.

3.2 X-ray crystal analysis

An appropriate crystal was cut from a larger one and mounted on a Kuma KM4 diffractometer equipped with a CCD counter. The collected data were corrected for polarization, Lorentz and absorption, the latter calculated from the crystal habits captured from photo scans. The positions of Eu were found from Patterson maps and the remainder of non-H atoms from difference Fourier maps. Positions of the C- and N-bonded hydrogen atoms were calculated geometrically. It was found that three water molecules and two guanidinium cations in **I**, and 1.5 H_2O molecules in **II** were disordered. The final refinements were anisotropic for all ordered non-H atoms, whereas the disordered C, N and O atoms were treated isotropically. The refinement was full matrix with all non-H atoms anisotropic. All computations were performed using SHELXS97 and SHELXL97 programs.[35,36] Molecular graphics were prepared with XP–Interactive Molecular Graphics.[37]

$[C(NH_2)_3]_5[Eu(DOTP)]\cdot 12.5H_2O$ (**I**) – $C_{17}H_{79}EuN_{19}O_{24.50}P_4$, M = 1184.52, monoclinic, space group P2/n, Z = 8, a = 26.576(2), b = 14.451(2), c = 27.285(2) Å, β = 111.21(4)°, V = 9768.2(8) Å^3, μ = 1.51 mm^{-1}, D_c = 1.656 g cm^{-3}, F(000) = 5064, crystal size = 0.43 × 0.23 × 0.21 mm, θ = 3–29°, index ranges: $-35 \le h \le 33$, $-19 \le k \le 19$, $-30 \le l \le 36$, reflections collected/unique = 66 186/23 210 (R_{int} = 0.0400). Final R indices [$I > 2\sigma(I)$] $R(F)$ = 0.0518, $R_w(F^2)$ = 0.1507 and $R(F)$ = 0.0628, $R_w(F^2)$ = 0.1627 (all data). Data completeness to 2θ = 28.78°, 99.06%. Largest differential peak and hole 4.337 and −2.405 e Å^{-3}. CCDC 1484638.

$K_5[Eu(DOTP)]\cdot 11H_2O$ (**II**) – $C_{12}H_{46}EuK_5N_4O_{23}P_4$, M = 1063.67, tetragonal, space group $P4cc$, Z = 4, a = 12.5231(10), b = 12.5231(10), c = 24.8781(4) Å, V = 3901.58(8) Å^3, μ = 2.39 mm^{-1}, D_c = 1.849 g cm^{-3}, F(000) = 2192, crystal size = 0.24 × 0.13 × 0.09 mm, θ = 3–29° index ranges: $-15 \le h \le 16$, $-15 \le k \le 16$, $-33 \le l \le 33$, reflections collected/unique = 29 178/4869 (R_{int} = 0.0368). Final R indices [$I > 2\sigma(I)$] $R(F)$ = 0.0447, $R_w(F^2)$ = 0.1340 and $R(F)$ = 0.0532, $R_w(F^2)$ = 0.1399 (all data). Data completeness to 2θ = 28.74°, 97.5%. Largest differential peak and hole 1.960 and −0.855 e Å^{-3}. CCDC 1484639.

3.3 Spectroscopic analysis

IR spectra were recorded with a Bruker IF S66 spectrometer. The spectra of crystalline complexes in KBr pellets and nujol suspension were recorded in the range of 50–4000 cm^{-1}. Electronic absorption spectra were recorded with a Cary 500 UV/Vis/NIR spectrophotometer. The corrected emission spectra were recorded with an Edinburgh Instruments FLS 920 spectrofluorometer.

3.4 Theoretical calculations

Vibrational frequencies of $\{K_4[Eu(DOTP)]\}^-$ clusters representing $\mathbf{II_{Eu1}}$ and $\mathbf{II_{Eu2}}$ sites were obtained *via* the DFT approach for the B3LYP exchange–correlation functional. The Eu ion was represented by the quasi-relativistic effective core potential (ECP) created by Dolg *et al.*,[38] along with the valence basis set [5s4p3d]-GTO. Remaining atoms, C, N, O, P, K, H, were represented by the 6-31G* basis set. Both structures of the $\{K_4[Eu(DOTP)]\}^-$ cluster were optimized (in vacuum) and harmonic vibrational frequencies were calculated for their optimized structures. Cartesian coordinates of the optimized geometries of $\{K_4[Eu(DOTP)]\}^-$ cluster are listed in Table S3 of the ESI.†

Energy levels were obtained *via ab initio* calculations based on the multireference wave function approach. These single-point calculations were performed for the two clusters $\{K_4[Eu(DOTP)]\}^-$ representing two different Eu sites of $K_5[Eu(DOTP)]\cdot 11H_2O$ crystal. *Ab initio* model potentials (AIMP) were used to represent the [Kr]-core of Eu ion closed shells along with the valence basis set of Gaussian-type orbitals (14s10p10d8f3g) contracted to obtain the [6s5p6d4f3g] basis set.[39] For the remaining atoms of the considered system, C, N, O, P, K, the AIMP effective core potentials along with valence Gaussian-type basis sets follow:[40]

- O: [He]-core, (5s6p1d)/[2s4p1d] basis set
- N: [He]-core, (5s5p1d)/[2s3p1d] basis set
- P: [Ne]-core, (7s6p1d)/[2s3p1d] basis set
- C: [He]-core, (5s5p1d)/[2s3p1d] basis set
- K: [Mg]-core, (9s7p)/[2s3p] basis set

In the case of H atoms, the 6-31G* basis set was used.[41] All effective core potentials account for mass-velocity and Darwin relativistic corrections by means of Cowan–Griffin approach.[42] The calculations were performed within C_2 symmetry with the MOLCAS package.[43]

The open-shell character of the Eu^{3+} ion ([Xe]4f^6 configuration) causes strong non-dynamic correlations effects. In this work the non-dynamic effects of electron correlation were taken into account within complete active space self-consistent field method (CASSCF),[18] where the active space was set by distributing six electrons onto one molecular orbital (MO) of a symmetry, two MOs of b symmetry and four MOs of e symmetry; all seven MOs defining the active space were predominantly of the Eu^{3+} ion 4f character. The molecular orbitals were optimized within separate state average (SA) CASSCF calculations minimizing the average energy of the following sets of spin-free states: one ^{7}A and two ^{7}B states; four ^{7}E; 19 ^{5}A and 20 ^{5}B states; and 38 ^{5}E states. In this way the following states of 4f^6 for the Eu^{3+} ion were taken into account: ^{7}F, ^{5}D, ^{5}L, ^{5}G, ^{5}H, ^{5}F, ^{5}I and ^{5}K. The effects of dynamical electron correlation were taken into account *via* second-order correction to the energy obtained within complete active space perturbation theory CASPT2.[19,20] In this work the multistate (MS) CASPT2[19,20] approach was used for the same sets of states as in the case of SA-CASSCF calculations. IPEA shift was set to zero.[44] In order to avoid the effect of so-called weak intruder states, the imaginary shift of 0.1 a.u. value was applied. Since the main interest of the present work is focused on low-lying states of the 4f^6 configuration of the Eu^{3+} ion, accounting for dynamical effects is limited to the central ion by means of the AFREeze option in the MOLCAS "caspt2" program, where inactive molecular orbitals with density on the Eu ion smaller than 0.1 were kept frozen during the MS-CASPT2 calculations. As a result, only three occupied orbitals localized on oxygens non-bonded to the Eu ion were correlated explicitly by means of the CASPT2

method. Cholesky decomposition[45] was performed for the matrix of the electron repulsion integrals with the threshold 10^{-8} Hartree, and consequently used thoroughout each step of calculations. In fact, just-mentioned approximations made these calculations tractable considering the particular choice of active space and accessible computational resources. Spin–orbit interaction was taken into account *via* the RASSI-SO approach,[21] where the matrix of the Hamiltonian including spin–orbit operator (coming from Douglas–Kroll Hamiltonian) over all considered above, MS-CASPT2 spin-free mixed states were constructed and diagonalized.

Acknowledgements

This work was supported by Wrocław University (grant 2178/W/WCH/09). A. K. acknowledges financial support from the Polish Ministry of Science and Higher Education (research project N N202 187636). A. K. also thanks Prof. Marek Krośnicki from the Institute of Theoretical Physics and Astrophysics, Gdańsk University, Poland, and Prof. Zoila Barandiaran and Prof. Luis Seijo from the Departamento de Química, Universidad Autónoma de Madrid, Spain, for discussions concerning calculations performed within the wave function-based multireference methods of quantum chemistry. Finally, computational time at the computing center of Institute of Theoretical Physics and Astrophysics, Gdańsk University, Poland, is acknowledged.

References

1 A. Merbach, L. Helm and E. Toth, *The Chemistry of Contrast Agents in Medical Magnetic Resonance Imaging*, John Wiley & Sons, Ltd, 2013.
2 (*a*) A. D. Sherry, J. Ren, J. Huskens, E. Brücher, É. Tóth, C. F. C. G. Geraldes, M. M. C. A. Castro and W. P. Cacheris, *Inorg. Chem.*, 1996, **35**, 4604–4612; (*b*) P. M. Winter and N. Bansal, *Magn. Reson. Med.*, 2001, **45**, 436–442.
3 (*a*) E. J. New, D. Parker, D. G. Smith and J. W. Walton, *Curr. Opin. Chem. Biol.*, 2010, **14**, 238–246; (*b*) J. C. G. Bünzli and S. V. Eliseeva, *Chem. Sci.*, 2013, **4**, 1939–1949; (*c*) S. J. Butler, M. Delbianco, L. Lamarque, B. K. McMahon, E. R. Neil, R. Pal, D. Parker, J. W. Walton and J. M. Zwier, *Dalton Trans.*, 2015, 4791–4803; (*d*) J. C. Bünzli, *J. Lumin.*, 2016, **170**, 866–878.
4 (*a*) J. D. Rinehart and J. R. Long, *Chem. Sci.*, 2011, **2**, 2078–2085; (*b*) J. Luzon and R. Sessoli, *Dalton Trans.*, 2012, **41**, 13556–13567; (*c*) G. Cucinotta, M. Perfetti, J. Luzon, M. Etienne, P.-E. Car, A. Caneschi, G. Calvez, K. Bernot and R. Sessoli, *Angew. Chem., Int. Ed.*, 2012, **51**, 1606–1610.
5 (*a*) L. Smentek, B. A. Hess, Jr., J. P. Cross, H. C. Manning and D. J. Bornhop, *J. Chem. Phys.*, 2005, **123**, 244302; (*b*) B. A. Hess, Jr, A. Kędziorski, L. Smentek and D. J. Bornhop, *J. Phys. Chem. A*, 2008, **112**, 2397–2407; (*c*) M. Purgel, Z. Baranyai, A. de Blas, T. Rodríguez-Blas, I. Bányai, C. Platas-Iglesias and I. Tóth, *Inorg. Chem.*, 2010, **49**, 4370–4382; (*d*) L. Smentek, *J. Phys.: Condens. Matter*, 2011, **23**, 143202; (*e*) C. Platas-Iglesias, A. Roca-Sabio, M. Regueiro-Figueroa, D. Esteban-Gómez, A. de Blas and T. Rodríguez-Blas, *Curr. Inorg. Chem.*, 2011, **1**, 91–116; (*f*) A. Roca-Sabio, M. Regueiro-Figueroa, D. Esteban-Gómez, A. de Blas, T. Rodríguez-Blas and C. Platas-Iglesias, *Comp. Theor. Chem.*, 2012, **999**, 93–104; (*g*) C. Platas-Iglesias, *Eur. J. Inorg. Chem.*, 2012, 2023–2033; (*h*) M. Regueiro-Figueroa, D. Esteban-Gomez, A. de Blas, T. Rodri guez-Blas and C. Platas-Iglesias, *Chem. – Eur. J.*, 2014, **20**, 3974–3981.
6 C. Görller-Walrand and K. Binnemans, in *Handbook of the Physics and Chemistry of Rare Earths*, ed. K. A. Gschneidner, Jr. and L. Eyring, Elsevier, Amsterdam, 1996, vol. 23.
7 F. Avecilla, J. A. Peters and C. F. G. C. Geraldes, *Eur. J. Inorg. Chem.*, 2003, 4179–4186.
8 E. F. Paulus, P. Juretschke and J. Lang, *Jahrestag der Deutschen Gesellschaft für Kristallographie*, Darmstadt, 1995.
9 (*a*) A. Mondry and R. Janicki, *Dalton Trans.*, 2006, 4702–4710; (*b*) R. Janicki and A. Mondry, *Polyhedron*, 2008, **27**, 1942–1946; (*c*) R. Janicki and A. Mondry, *Eur. J. Inorg. Chem.*, 2013, 3429–3438; (*d*) R. Janicki, M. Monteil, M. Lecouvey and A. Mondry, *Opt. Mater.*, 2013, **36**, 259–264.
10 J. Gałęzowska, R. Janicki, A. Mondry, R. Burgada, T. Bailly, M. Lecouvey and H. Kozłowski, *Dalton Trans.*, 2006, 4384–4394.
11 (*a*) M. R. Spirlet, J. Rebizant, J. F. Desreux and M. F. Loncin, *Inorg. Chem.*, 1984, **23**, 359–363; (*b*) F. Benetollo, G. Bombieri, S. Aime and M. Botta, *Acta Crystallogr., Sect. C: Cryst. Struct. Commun.*, 1999, **55**, 353–356.
12 K. M. Payne, E. J. Valente, S. Aime, M. Botta and M. Woods, *Chem. Commun.*, 2013, **49**, 2320–2322.
13 (*a*) S. Aime, M. Botta, E. Terreno, P. L. Anelli and F. Uggeri, *Magn. Reson. Med.*, 1993, **30**, 583–591; (*b*) R. A. Carvalhoa, J. A. Petersc and C. F. G. C. Geraldesa, *Inorg. Chim. Acta*, 1997, **262**, 167–176; (*c*) Z. Kotková, G. A. Pereira, K. Djanashvili, J. Kotek, J. Rudovský, P. Hermann, L. Vander Elst, R. N. Muller, C. F. G. C. Geraldes, I. Lukes and J. A. Peters, *Eur. J. Inorg. Chem.*, 2009, 119–136; (*d*) G. A. Pereira, L. Ball, A. D. Sherry, J. A. Peters and C. F. G. C. Geraldes, *Helv. Chim. Acta*, 2009, **92**, 2532–2551.
14 B. R. Judd, *Phys. Rev.*, 1962, **127**, 750–761.
15 G. S. Ofelt, *J. Chem. Phys.*, 1962, **37**, 511–519.
16 P. A. Tanner, *Chem. Soc. Rev.*, 2013, **42**, 5090–5101.
17 A. Kędziorski and L. Smentek, *J. Lumin.*, 2007, **127**, 552–560.
18 (*a*) B. O. Roos, P. R. Taylor and P. E. M. Siegbahn, *Chem. Phys.*, 1980, **48**, 157–173; (*b*) P. E. M. Siegbahn, A. Heiberg, B. O. Roos and B. Levy, *Phys. Scr.*, 1980, **21**, 323–327; (*c*) P. E. M. Siegbahn, A. Heiberg, J. Almlöf and B. O. Roos, *J. Chem. Phys.*, 1981, **74**, 2384–2396.
19 (*a*) K. Andersson, P.-Å. Malmqvist, B. O. Roos, A. J. Sadlej and K. Wolinski, *J. Phys. Chem.*, 1990, **94**, 5483–5488; (*b*) K. Andersson, P.-Å. Malmqvist and B. O. Roos, *J. Chem. Phys.*, 1992, **96**, 1218–1226.
20 J. Finley, P.-Å. Malmqvist, B. O. Roos and L. Serrano-Andrés, *Chem. Phys. Lett.*, 1998, **288**, 299–306.
21 P. Å. Malmqvist, B. O. Roos and B. Schimmelpfennig, *Chem. Phys. Lett.*, 2002, **357**, 230–240.
22 (*a*) F. Serpaggi, G. FeHrey and E. Antic-Fidancev, *J. Solid State Chem.*, 1999, **148**, 347–352; (*b*) J.-G. Mao, *Coord. Chem. Rev.*, 2007, **251**, 1493–1520.

23 M. Krośnicki, A. Kędziorski, L. Seijo and Z. Barandiarán, *J. Phys. Chem. A*, 2014, **118**, 358–368.
24 W. T. Carnall, P. R. Fields and K. Rajnak, *J. Chem. Phys.*, 1968, **49**, 4450–4455.
25 M. Seth, K. G. Dyall, R. Shepard and A. Wagner, *J. Phys. B: At., Mol. Opt. Phys.*, 2001, **34**, 2383–2406.
26 C. Holzer, A. M. Wernbacher, J. M. Senekowitsch, K. Gatterer and A. M. Kelterer, *J. Phys. Chem. A*, 2014, **118**, 1149–11511.
27 A. Kramida, Yu. Ralchenko, J. Reader and NIST ASD Team (2015). NIST Atomic Spectra Database (ver. 5.3), [Online]. Available: http://physics.nist.gov/asd [2016, April 28]. National Institute of Standards and Technology, Gaithersburg, MD.
28 Z. Barandiarán and L. Seijo, *J. Chem. Phys.*, 2013, **138**, 074102.
29 (*a*) M. Albin and W. D. Horrocks Jr., *Inorg. Chem.*, 1985, **24**, 895–900; (*b*) S. T. Frey and W. D. Horrocks Jr., *Inorg. Chim. Acta*, 1995, **229**, 383–390; (*c*) G. R. Choppin and Z. M. Wang, *Inorg. Chem.*, 1997, **36**, 249–252.
30 (*a*) H. D. Amberger, H. Reddmann and C. Hagen, *Inorg. Chim. Acta*, 2005, **358**, 3745–3752; (*b*) P. A. Tanner, Y. Y. Yeung and L. Ning, *J. Phys. Chem.*, 2013, **117**, 2771–2781.
31 S. P. Sinha and H.-H. Schmidtke, *Mol. Phys.*, 1965, **10**, 7–11.
32 A. Kędziorski, in preparation.
33 P. A. Tanner, Y. Y. Yeung and L. Ning, *J. Phys. Chem. A*, 2013, **117**, 2771–2781.
34 R. Janicki, A. Kędziorski and A. Mondry, in preparation.
35 G. M. Sheldrick, *SHELXS-97, program for structure solution*, University of Göttingen, 1997.
36 G. M. Sheldrick, *SHELXL-97, program for structure refinement*, University of Göttingen, 1997.
37 40 XP-Interactive Molecular Graphics, v. 5.1–Bruker Analytical X-ray Systems 1998.
38 M. Dolg, H. Stoll, A. Savin and H. Preuss, *Theor. Chim. Acta*, 1989, **75**, 173.
39 L. Seijo, Z. Barandiarán and B. Ordejon, *Mol. Phys.*, 2003, **101**, 73.
40 Z. Barandiarán and L. Seijo, *Can. J. Chem.*, 1992, **70**, 409.
41 P. C. Hariharan and J. A. Pople, *Theor. Chim. Acta*, 1973, **28**, 213.
42 R. D. Cowan and D. C. Griffin, *J. Opt. Soc. Am.*, 1976, **66**, 1010.
43 (*a*) F. Aquilante, L. De Vico, N. Ferré, G. Ghigo, P.-Å. Malmqvist, P. Neogrády, T. B. Pedersen, M. Pitonak, M. Reiher, B. O. Roos, L. Serrano-Andrés, M. Urban, V. Veryazov and R. Lindh, *J. Comput. Chem.*, 2010, **31**, 224; (*b*) V. Veryazov, P.-O. Widmark, L. Serrano-Andres, R. Lindh and B. O. Roos, *Int. J. Quantum Chem.*, 2004, **100**, 626; (*c*) G. Karlström, R. Lindh, P.-Å. Malmqvist, B. O. Roos, U. Ryde, V. Veryazov, P.-O. Widmark, M. Cossi, B. Schimmelpfennig, P. Neogrády and L. Seijo, *Comput. Mater. Sci.*, 2003, **28**, 222.
44 G. Ghigo, B. O. Roos and P. Å. Malmqvist., *Chem. Phys. Lett.*, 2004, **396**, 142.
45 F. Aquilante, L. Boman, J. Boström, H. Koch, R. Lindh, A. S. de Merás and T. B. Pedersen in *Challenges and Advances in Computational Chemistry and Physics*, ed. R. Zalesny, M. G. Papadopoulos, Mezey, G. Paul and J. Leszczynski, Springer Science + Business Media B.V., 2011, vol. 13, pp. 301–343.